PERGAMON International Journal of Multiphase Flow 25 (1999) 1619–1643

International Journal of Multiphase Flow

www.elsevier.com/locate/ijmulflow

Grid-averaged Lagrangian LES model for multiphase turbulent flow

Kazuo Nadaoka*, Yasuo Nihei, Hiroshi Yagi

Department of Mechanical and Environmental Informatics, Graduate School of Information, Science and Engineering, Tokyo Institute of Technology, 2-12-1 O-okayama, Meguro-ku, Tokyo, 152-8552, Japan

Received 17 August 1998; received in revised form 24 November 1998

Abstract

A grid-averaged Lagrangian (GAL) model for dispersed particle motion in multiphase turbulent flow is presented to provide a large eddy simulation (LES) model for multiphase turbulent flow in which a quite large number of particles are involved. The GAL model is based on an averaging operation for a Lagrangian-type equation of motion of a particle over a computational grid volume and a procedure of reallocation of a dispersed particle cloud with its centroid movement to each grid. The model is therefore a mixed Eulerian–Lagrangian model which can effectively reduce computational time compared with existing Lagrangian-type models, without losing the advantage of Lagrangian-type models that they can properly describe the dynamical evolution of particles. Since the GAL model adopts the grid-volume averaging operation it can easily provide an effective SGS model for LES modeling of multiphase turbulent flow. The validity of the multiphase LES model developed, which is named the GAL-LES model, is confirmed through its application to a particle plume, in which the present model is found to simulate large-eddy motion usually observed in a jet and plume, and to give good agreements with experimental data. © 1999 Elsevier Science Ltd. All rights reserved.

Keywords: Large eddy simulation; Multiphase turbulent flow; GAL model; Numerical simulation; Particle plume; Mixed Eulerian–Lagrangian model

1. Introduction

Multiphase turbulent flow is observed in many situations of interest in civil, chemical and mechanical engineering and others. In particular, multiphase flows encountered in civil

* Corresponding author. Tel.: +81-3-5734-2589; fax: +81-3-5734-2650.
E-mail address: nadaoka@mei.titech.ac.jp (K. Nadaoka)

0301-9322/99/$ - see front matter © 1999 Elsevier Science Ltd. All rights reserved.
PII: S0301-9322(98)00079-2

engineering, such as sediment transport in rivers and coasts, debris flow and pyroclastic flow, are characterized as large-scale motions with a quite large number of particles. Although many experiments on such flows have been conducted, the difficulty in measuring the velocity field of each phase and the particle concentration prevents us from understanding the physical processes therein. On the other hand, the recent progress in computer performance has increased the potential for numerically simulating these flows.

Existing turbulence models for multiphase flow are based on mostly time-averaged formulations, similar to the two-equation models for single-phase turbulent flow (e.g. Elghobashi and Abou-Arab, 1983; Chen and Wood, 1985). These multiphase turbulence models contain many parameters to be tuned for each specific multiphase flow. Furthermore it is not easy to apply them to multiphase flow with strong non-uniformity both in time and space, such as plug flow. Although numerical simulation of multiphase turbulent flow is performed also with DNS: direct numerical simulation (e.g. Squires and Eaton, 1990), it is difficult to apply DNS to multiphase flows under high Reynolds number condition owing to its heavy computational load.

For further progress in multiphase flow study, it is desirable to develop a LES (large eddy simulation)-type turbulence model, which contains a smaller number of model parameters and may simulate considerably non-uniform or eddying multiphase flow. There have been some attempts at LES computation of a dilute suspension using the Smagorinsky model for SGS (sub-grid scale) turbulence (e.g. Ebert and Dehning, 1992). However for multiphase flow with a quite large number of particles no effective SGS model has been developed, mainly because of the lack of a reasonable formulation of the dispersed-particle motion. Therefore the crucial point for the development of multiphase LES model is to provide a new formulation of the dispersed-particle motion under more general conditions.

A classification of the previous models for dispersed-particle motion is represented in Fig. 1, where the Lagrangian- and Eulerian-type models are separately categorized. The former is further classified into the hard-particle model, DEM (discrete element method) and DSMC (direct simulation Monte Carlo) method according to the difference in the treatment of interactions between particles. The hard-particle model is based on a direct treatment of instantaneous contacts between particles and hence can accurately predict the motion of solid

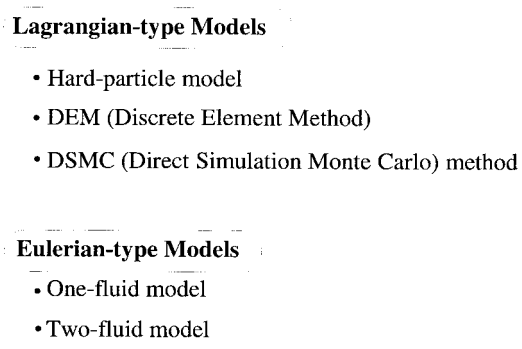

Fig. 1. Classification of the previous models for dispersed-particle motion.

particles (Campbell and Brennen, 1985). However, this model has to bear the heaviest computational load among the models shown in Fig. 1, because a very short time step is required for accurate calculation of the collisions between particles. Therefore this model is not suitable for practical applications, in which computation for a quite large number of particles is needed. The DEM introduced by Cundall (1971), on the other hand, treats one or several particles as an element and traces each element in time, considering the interaction between elements based on a simple model with springs and dash-pots. The DEM has been applied to various flows including large-scale multiphase flow such as debris flow (e.g. Uchida and Hakuno, 1990), because the CPU time can be effectively reduced. However the computational results are of doubtful accuracy because it is difficult to determine accurately the stiffness and damping coefficients in the spring and dash-pot models. The DSMC method, which was developed by Bird (1976) for solving the equations of rarefied gas dynamics, has been applied to gas–solid phase flow by Kitron et al. (1990) and Tanaka et al. (1991). The model is conceptually stochastic and therefore computationally very efficient and can be applied to multiphase flow with a large number of particles. However, since this method adopts an operator-splitting technique, by which particle motion is divided into free movement and collisions, it cannot in principle be applied to multiphase flow with dense particle layers, where continuous contacts between particles exist.

The Eulerian-type models, which treat the dispersed-particle phase as a continuous medium, are classified into one-fluid model and two-fluid model (e.g. Marble, 1970). Generally they need shorter CPU times and less memory size than the Lagrangian-type models. Although this is a big advantage for calculating large-scale multiphase flows, it is difficult for the Eulerian-type models to theoretically derive constitutive laws for the dispersed-particle motion in a manner reflecting the physical processes concerned. Therefore various empirical equations are to be used for the constitutive laws.

From these considerations it is expected that, as one of the possible and promising ways to yield a reasonable formulation of dispersed-particle motion with a proper physical background as well as computational efficiency, one may employ a mixed Eulerian–Lagrangian approach. On this line, in the present study, a new model for dispersed particle motion in multiphase turbulent flow is presented to provide an LES model for multiphase turbulent flow in which a large number of particles are involved. The model for dispersive particle motion, which is referred to here as the GAL (grid-averaged Lagrangian) model, is based on an averaging operation for a Lagrangian-type equation of motion of a particle over a computational grid volume and a procedure of reallocation of a dispersed particle cloud with its centroid movement to each grid. The model is therefore a mixed Eulerian–Lagrangian model which can effectively reduce computational time compared with existing Lagrangian-type models, without losing the advantage of Lagrangian models that they can properly describe the dynamical evolution of particles. Since the GAL model adopts the grid-volume averaging operation it can easily provide an effective SGS model for LES modeling of multiphase turbulent flow. The validity of the multiphase LES model developed, which is named the GAL-LES model, is confirmed through its application to a particle plume, in which the present model is found to simulate large-eddy motion usually observed in a jet and plume, and give good agreements with the experimental data by Tamai and Muraoka (1996). (The preliminary GAL-LES model is outlined in Nadaoka et al., 1995.)

2. GAL-LES model

2.1. Outline of the GAL model for particle motion

As schematically shown in Fig. 2a, a cloud of particles located in a grid volume at time t may be advected with its deformation and diffusion during a time interval Δt under the combined action of the various forces acting on the particles. A complete description of the cloud evolution needs to trace the motion of all the particles in the cloud. Computationally, however, this is a formidable task when the total number of particles becomes very large.

To reduce the computational time, in the GAL model, the cloud motion is represented by the two components, i.e. the movement of the centroid of the particle cloud, and the particle variances around it in each coordinate direction as shown in Fig. 2b. These two components can be evaluated, as shown later, with the Lagrangian-type equations for the particle movements averaged over all the particles located in a grid volume at time t. Since the expansion of the particle cloud so simplified may be easily calculated from the equation for the particle velocity variance, the particle concentration of the cloud at $t+\Delta t$ is also readily

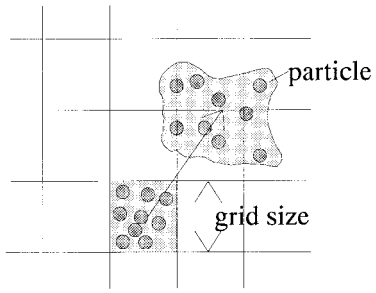

(a) Actual cloud movement

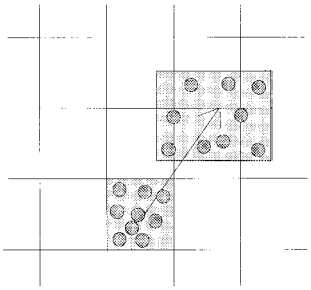

(b) Simplification in the GAL model

Fig. 2. Schematic illustration of the evolution of a particle cloud in a grid volume during a time interval Δt and its simplification in the GAL model. (a) Actual cloud movement. (b) Simplification in the GAL model.

evaluated, and its value, with the contributions from all other clouds, can be reallocated to each grid volume in a geometrical manner. These values in each grid volume, together with other variables like velocities, may be used to calculate the grid-averaged and fluctuating particle movements at the next time step. The grid-averaged values will also be used for the Eulerian LES computation of the fluid-phase motion. Therefore the complete procedure is a mixed Eulerian–Lagrangian approach, and is summarized as follows:

1. The stochastic differential equations of the grid-averaged particle velocity and velocity variance, which will be described below, are integrated from t to $t+\Delta t$ for the particle cloud located in each grid volume at time t.
2. With the evolved grid-averaged particle velocity and velocity variance the centroid movement and cloud expansion of each particle cloud during Δt are calculated.
3. Contributions of the grid-averaged particle velocity and variance and the particle concentration from all the particle clouds at $t+\Delta t$ are collected and reallocated to each grid.

2.2. Equations for particle motion in the GAL model

In the GAL model particle motion is represented with its grid-averaged particle velocity and variance. These quantities, as derived below, are obtained by averaging the Lagrangian-type equation of the particle movement over all the particles in each grid volume.

Denoting the particle velocity component in the x_i direction (i = 1, 2, 3) u_{si}, the equation of motion of a particle with diameter d and density ρ_s is given as

$$\rho_s \frac{\pi d^3}{6} \frac{\mathrm{d}u_{si}}{\mathrm{d}t} = F_{Di} + F_{Li} + F_{Mi} + F_{Pi} + F_{Gi} + F_{Ci} \tag{1}$$

where the forces on the right-hand side are respectively the drag, lift, inertia force of virtual mass, fluid pressure gradient, buoyancy and the forces between particles. The Basset history term is neglected. These forces are evaluated as follows. The drag force is given by

$$F_{Di} = C_D \frac{\rho}{2} \frac{\pi d^2}{4} u_{ri} \mid u_{rj} \mid \tag{2}$$

where ρ denotes the fluid density and $u_{ri}(=u_i - u_{si})$ represents the relative velocity between the fluid and the particle, u_i being the fluid velocity. The drag coefficient C_D is chosen to allow for a wide range variation in particle concentration c (Bouillard et al., 1989):

$$C_D = \frac{24}{R_{ed}}(1 + 0.15R_{ed})^{0.687}(1-c)^{-2.7} \tag{3}$$

where $R_{ed}(=|u_{ri}|\mathrm{d}/\nu)$ is the particle Reynolds number and ν is the kinematic fluid viscosity.

The lift force is expressed as a function of the vorticity of the fluid phase ω_i:

$$F_{Li} = C_L \rho \frac{\pi d^3}{6} \varepsilon_{ijk} u_{rj} \omega_k \tag{4}$$

which is in line with Auton et al. (1988). In Eq. (4), the lift coefficient C_L is taken as a constant of 0.03.

The forces due to fluid pressure gradient and virtual inertia are formulated by following Auton et al. (1988),

$$F_{Pi} = \rho \frac{\pi d^3}{6} \frac{Du_i}{Dt} \tag{5}$$

$$F_{Mi} = \rho C_m \frac{\pi d^3}{6} \left(\frac{Du_i}{Dt} - \frac{du_{si}}{dt} \right) \tag{6}$$

where C_m is the virtual mass coefficient ($=0.50$) and D/D_t denotes the substantial differentiation. The buoyancy force is given as follows:

$$F_{Gi} = -(\rho_s - \rho) \frac{\pi d^3}{6} \boldsymbol{g} \delta_{i2} \tag{7}$$

where $\boldsymbol{g}$ is the gravitational acceleration in the $-x_2$ direction.

The inter-particle force, F_C, which is a dominant factor in multiphase flow with high particle concentration, is neglected in the present description of the model. The GAL model may rationally evaluate this force by considering the physical aspects of particle collisions and contacts from the Lagrangian-type equation for the particle motion. However the modeling of the inter-particle force is a challenging but difficult research theme of multiphase flow. Since the principal purpose of the present study is to provide a basic framework for the multiphase LES, the inter-particle force is neglected for the present. (Its preliminary modeling was presented by Nihei et al., 1997).

The particle and fluid velocities and the particle concentration are separated into grid-averaged and fluctuating components, denoted by an overbar and a prime, respectively:

$$u_{si} = \overline{u_{si}} + u'_{si}$$

$$u_i = \overline{u_i} + u'_i$$

$$c = \bar{c} + c' \tag{8}$$

The equations of the grid-averaged particle velocity are derived by substituting Eq. (8) into Eqs. (1)–(7) and averaging over each grid volume. Assuming that the grid-averaged component of the particle concentration is much greater than the fluctuating component, we can describe the equations of the grid-averaged particle velocity as

$$\frac{\mathrm{d}\overline{u_{si}}}{\mathrm{d}t} = \frac{\rho}{\rho_s + \rho C_m}\left[\frac{18\nu}{d^2}(1+0.15R_{ed}^*)^{0.687}(1-\bar{c})^{-2.7}\overline{u_{ri}} + C_L\varepsilon_{ijk}\overline{u_{rj}\omega_k} + (1+C_m)\frac{\mathrm{D}\overline{u_i}}{\mathrm{D}t} - \left(\frac{\rho_s}{\rho}-1\right)\boldsymbol{g}\delta_{i2}\right] \tag{9}$$

where the grid-averaged value is used for the relative velocity between the fluid and the particle in R_{ed}^* and $\mathrm{D}\overline{u_i}/\mathrm{D}t = \partial\overline{u_i}/\partial t + \overline{u_j}\partial\overline{u_i}/\partial x_j$.

The equation of the particle-velocity variance is derived from the equations of the fluctuating component of the particle motion obtained by Tchen (1947)'s assumptions, with a formulation of spectral response of a particle to the agitation by SGS turbulence according to Hinze (1975). The equations are given by subtracting Eq. (9) from Eq. (1) and neglecting higher order nonlinear terms,

$$\frac{\mathrm{d}u'_{si}}{\mathrm{d}t} = \frac{\rho}{\rho_s + \rho C_m}\left[\frac{18\nu}{d^2}(1+0.15R_{ed}^*)^{0.687}(1-\bar{c})^{-2.7}u'_{ri} + (1+C_m)\frac{\partial u'_i}{\partial t}\right] \tag{10}$$

where the first term in the right-hand side corresponds to the fluctuating component of the drag, and the second term to the inertia force of virtual mass and fluid pressure gradient. In Eq. (10), the fluctuating lift force is neglected because of the lack of its reasonable formulation. Eq. (10) may be re-arranged into the following form:

$$A_1 u'_{si} + \frac{\mathrm{d}u'_{si}}{\mathrm{d}t} = A_1 u'_i + A_2\frac{\partial u'_i}{\partial t} \tag{11}$$

where

$$A_1 = \frac{\rho}{\rho_s + \rho C_m}\frac{18\nu}{d^2}(1+0.15R_{ed}^*)^{0.687}(1-\bar{c})^{-2.7}, \quad A_2 = \frac{\rho(1+C_m)}{\rho_s + \rho C_m} \tag{12}$$

The spectral transformation of Eq. (11) yields

$$S_{pp}(\omega^*) = \frac{A_1^2 + A_2^2\omega^{*2}}{A_1^2 + \omega^{*2}}S_{ff}(\omega^*) \tag{13}$$

where $S_{pp}(\omega^*)$ and $S_{ff}(\omega^*)$ are the frequency spectra of the particle and fluid velocity fluctuation, respectively, and ω^* is the angular frequency of the fluctuation. In order to derive the equations for $\overline{u_{si}'^2}$ from Eq. (13), $S_{ff}(\omega^*)$ must be known. Unfortunately, however, its general form for multiphase turbulent flow is not obtained. Therefore, in the present model, Eq. (13) is simplified as

$$\overline{u_{si}'^2} = \frac{A_1^2 + A_2^2\omega_0^{*2}}{A_1^2 + \omega_0^{*2}}\overline{u_i'^2} \tag{14}$$

where ω_0^* is a representative frequency of the SGS turbulence and may be evaluated with the computational grid size Δ,

$$\omega_0^* = \frac{2\pi \mid \overline{u_i} \mid}{\Delta} \tag{15}$$

In a similar fashion, the following expression is adopted for $\overline{u_{si}' u_i'}$

$$\overline{u_{si}' u_i'} = \frac{A_1^2 + A_2 \omega_0^{*2}}{A_1^2 + \omega_0^{*2}} \overline{u_i'^2} \tag{16}$$

2.3. Particle-cloud evolution and reallocation procedure in the GAL model

The changes in the centroid position of a particle cloud $\Delta\overline{x_{si}}$ and its variance $\Delta\overline{x_{si}'^2}$ during the computational time interval Δt are obtained from the grid-averaged particle velocity and its variance,

$$\Delta\overline{x_{si}} = \overline{u_{si}}\Delta t \tag{17}$$

$$\Delta\overline{x_{si}'^2} = 2\overline{u_{si}'^2} T_s \Delta t \tag{18}$$

where T_s denotes a Lagrangian integral time scale for the particle motion and is regarded as the representative time for the diffusion process of the particle motion. Eq. (18) is derived by assuming that the variance of particle motion in the GAL model is governed by the SGS turbulence motion in the fluid phase, whose scale is smaller than that of the computational grid size. The previous results by DNS (e.g. Squires and Eaton, 1991) suggest that the Lagrangian velocity autocorrelations of the particle and surrounding fluid are different due to the effects of the particle inertia and cross-trajectory. To take account of these effects, T_s is given as

$$T_s = S_{iner} S_{cross} T_L \tag{19}$$

In the above equation, T_L represents a Lagrangian integral time scale for the fluid motion and is expressed according to Elghobashi et al. (1984),

$$T_L = \frac{5k}{12\varepsilon} \tag{20}$$

where k and ε are, respectively, the kinetic energy and the dissipation rate of the SGS turbulence in the fluid phase. S_{iner} and S_{cross} in Eq. (19) are introduced to incorporate respectively the particle inertia and cross-trajectory effects into T_s and are given by Mols and Oliemans (1998),

$$S_{iner} = 1 + \tau_p / T_L \tag{21}$$

$$S_{cross} = \frac{1}{\sqrt{1 + (\mid \overline{u_{ri}} \mid T_L/\Delta)^2}} \tag{22}$$

where τ_p represents the particle relaxation time. Eqs. (19)–(22) take account of only the

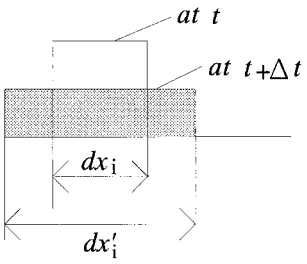

Fig. 3. Uniform probability distribution of the particle position in a grid volume (Nadaoka et al., 1995).

fluctuating forces between the two phases due to the SGS turbulence. For more general estimation of T_s the effects of the inter-particle forces should also be included in the formulation. This is however left for future studies.

The probability distribution of the particle position in a grid volume must be assumed for the reallocation operation. In the preceding preliminary study (Nadaoka et al., 1995), the uniform distribution as shown in Fig. 3 was adopted for the geometrical simplicity. The reallocation procedure based on the uniform distribution is illustrated in Fig. 4. The particle clouds located in the grid i, $i + 1$ and $i + 2$ at time t vary their centroid positions and sizes due to advection and diffusion during Δt, and the evolved particle clouds may be situated over a few grids in a mutually overlapping manner. Then at time $t+\Delta t$ all fractions from these particle clouds contributing to a grid are collected and reallocated to the grid with the uniform distribution in the grid. With this operation, however, a numerical diffusion may inevitably appear in the advection process. Fig. 5 exemplifies the numerical diffusion in a one-dimensional advection process generated by the above described operation; i.e. the particle cloud located in

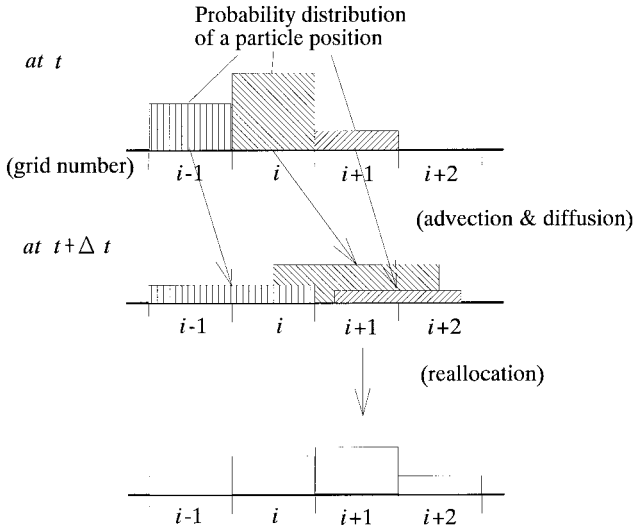

Fig. 4. Schematic illustation of the reallocation procedure based on the uniform distribution.

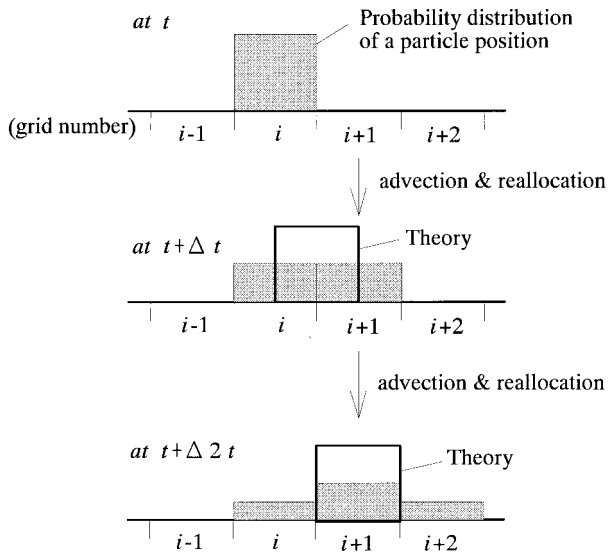

Fig. 5. Illustration of numerical diffusion in an advection process generated by the GAL model using the uniform probability distribution in the particle cloud.

the grid i at time t, due to the reallocation, results in the wider distributions around the theoretical distribution at the subsequent time steps.

To reduce the numerical diffusion, in the present study, an alternative method of reallocation has been employed. Instead of redistributing the collected fractions in a grid into a cloud with the uniform distribution, the centroid of these fractions in the grid is retained and a rectangular distribution around the centroid is given in the grid as the reallocation, as shown in Fig. 6. The width of the particle cloud in the grid j, $\mathrm{d}x(j)$, is represented with the relative position of the centroid, $x_s(j)$, and the grid center, $x_c(j)$:

$$x_s(j) < x_c(j)$$

$$\mathrm{d}x(j) = 2\{x_s(j) - 0.5[x_c(j) + x_c(j-1)]\}$$

$$x_s(j) > x_c(j)$$

$$\mathrm{d}x(j) = 2\{0.5[x_c(j+1) + x_c(j)] - x_s(j)\} \tag{23}$$

Fig. 7 shows the result by the modified reallocation procedure for the one-dimensional advection process, indicating that the reallocated particle cloud is in quite good agreement with the theoretical one.

With the rectangular distribution of a particle cloud in a grid volume, the expanded cloud size in the x_i-direction during Δt, $\mathrm{d}x_i'$, may be estimated with the squared size of the particle cloud at time t, $\mathrm{d}x_i^2$, and the change in the variance of particle position, $\Delta\overline{x_{si}'^2}$, as follows:

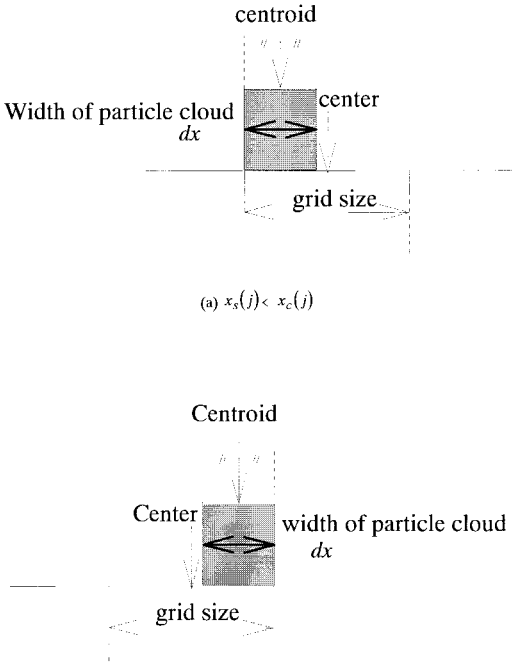

Fig. 6. Rectangular cloud distribution around the centroid for the improved reallocation procedure; $x_s(j)$: centroid; $x_c(j)$: grid center; (a) $x_s(j) < x_c(j)$; (b) $x_s(j) > x_c(j)$.

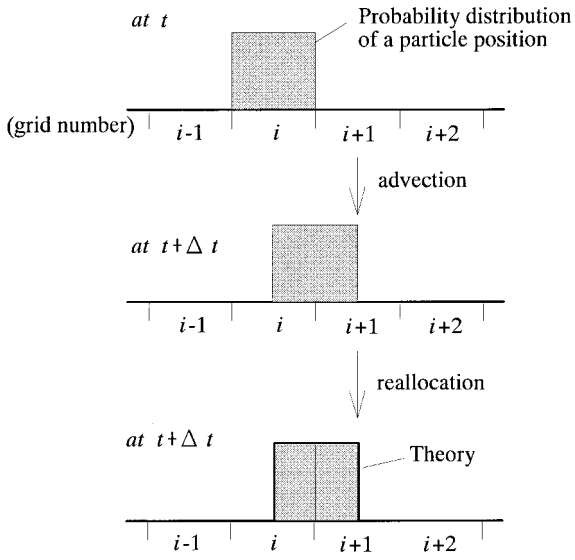

Fig. 7. Improved reallocation procedure for the one-dimensional advection process.

$$\mathrm{d}x_i'^2 = \mathrm{d}x_i^2 + 12\Delta\overline{x_{si}'^2} \tag{24}$$

The probability that a fraction of the particle cloud located in the grid i at time t is situated in the grid j after Δt, which is expressed as $f(i, j)$, must be evaluated for the reallocation. In Fig. 7, for example, $f(i, i) = 0.50$ and $f(i, i + 1) = 0.50$. Obviously for the conservation of the particle cloud volume $f(i, j)$ must satisfy the condition,

$$\sum_{j=1}^{i_{\max}} f(i,j) = 1 \tag{25}$$

where $i_{\max}$ is the total number of the computational grids. With $f(i, j)$ any quantities associated with the particle cloud in the grid j at time $t+\Delta t$ may be expressed by collecting the contributions from all the grids. For example, the particle concentration and velocity are given as

$$\overline{c^{n+1}(j)} = \sum_{i=1}^{i_{\max}} \overline{c^n(i)} f(i,j) \tag{26}$$

$$\overline{u_s^{n+1}(j)} = \sum_{i=1}^{i_{\max}} \overline{u_s^n(i)} \frac{\overline{c^n(i)} f(i,j)}{\overline{c^{n+1}(j)}} \tag{27}$$

where n and $n + 1$ denote the computational time steps corresponding to t and $t+\Delta t$, respectively. Likewise, the centroid of the particle cloud, $x_s(j)$, is expressed as

$$x_s^{n+1}(j) = \sum_{i=1}^{i_{\max}} x_s'^n(i,j) \frac{\overline{c^n(i)} f(i,j)}{c^{n+1}(j)} \tag{28}$$

where $x_s'^n(i, j)$ is the centroid of a fraction of particle cloud in the grid j at the time step $n + 1$ which is located in the grid i at the time step n.

The fundamental performance of the GAL model with this reallocation procedure has been examined by applying it to simple advection and diffusion processes for which exact analytical solutions exist. The computational results by the GAL model for simple one-dimensional advection and diffusion processes, as shown later in Section 3, indicate nearly perfect agreements with the analytical solutions.

2.4. Equations of the fluid-phase motion

The fluid-phase motion is formulated in a manner similar to that for the usual LES except for the inclusion of the particle concentration c and the interaction forces between the fluid and particles. The SGS turbulence is evaluated with an equation of turbulence kinetic energy k which includes the additional terms due to the forces between the two phases in GS and SGS component, P_G and P_S, respectively.

The continuity, momentum and turbulence kinetic energy equations are given as

$$\frac{\partial}{\partial t}(1-\bar{c})+\frac{\partial}{\partial x_i}\{\overline{u_i}(1-\bar{c})\}+\frac{\partial}{\partial x_i}\{-\overline{u_i'c'}\}=0 \tag{29}$$

$$\frac{\mathrm{D}\overline{u_i}}{\mathrm{D}t}=-\frac{1}{\rho}\frac{\partial \bar{p}}{\partial x_i}+\frac{\partial R_{ij}}{\partial x_j}-\frac{\bar{c}}{1-\bar{c}}\left[\frac{18\nu}{d^2}(1+0.15R_{ed}^{*})^{0.687}(1-\bar{c})^{-2.7}\overline{u_{ri}}+C_{\mathrm{L}}\varepsilon_{ijk}\overline{u_{rj}\omega_k}\right.$$
$$\left.+(1+C_{\mathrm{m}})\frac{\mathrm{D}\overline{u_i}}{\mathrm{D}t}-C_{\mathrm{m}}\frac{\mathrm{d}\overline{u_{si}}}{\mathrm{d}t}\right] \tag{30}$$

$$\frac{\mathrm{D}k}{\mathrm{D}t}=R_{ij}\frac{\partial \overline{u_i}}{\partial x_j}+\frac{\partial}{\partial x_i}\left(\nu_{\mathrm{t}}\frac{\partial k}{\partial x_i}\right)-C_{\mathrm{e}}\frac{k^{3/2}}{\Delta}+P_{\mathrm{S}}+P_{\mathrm{G}} \tag{31}$$

where

$$R_{ij}(=-\overline{u_i'u_j'})=\nu_{\mathrm{t}}\left(\frac{\partial \overline{u_i}}{\partial x_j}+\frac{\partial \overline{u_j}}{\partial x_i}\right)-\frac{2}{3}k\delta_{ij} \tag{32}$$

$$\nu_{\mathrm{t}}=C_{\mathrm{S}}k^{1/2}\Delta \tag{33}$$

$$\Delta=(\mathrm{d}x_1\ \mathrm{d}x_2\ \mathrm{d}x_3)^{1/3} \tag{34}$$

$$\overline{u_i'c'}=-\frac{\nu_{\mathrm{t}}}{\sigma_{\mathrm{c}}}\frac{\partial}{\partial x_i}(1-\bar{c}) \tag{35}$$

$$P_{\mathrm{S}}=\frac{\bar{c}}{1-\bar{c}}\left[\frac{18\nu}{d^2}(1+0.15R_{\mathrm{ed}})^{0.687}(1-\bar{c})^{-2.7}(\overline{u_{si}'u_i'}-2k)+\frac{1}{2}C_{\mathrm{m}}\frac{\mathrm{d}\overline{u_{si}'u_i'}}{\mathrm{d}t}-(1+C_{\mathrm{m}})\frac{\mathrm{D}k}{\mathrm{D}t}\right] \tag{36}$$

$$P_{\mathrm{G}}=\alpha\frac{\bar{c}}{1-\bar{c}}\frac{18\nu}{d^2}(1+0.15R_{\mathrm{ed}})^{0.687}(1-\bar{c})^{-2.7}\mid\overline{u_{\mathrm{r}j}}\mid^2 \tag{37}$$

In the above equations, ν_{t} denotes the SGS eddy viscosity and R_{ij} represents the Reynolds stress due to the SGS turbulence in the fluid-phase motion. The constant values usually adopted for LES are given for C_{s} and C_{e}; i.e. $C_{\mathrm{s}}=0.12$ and $C_{\mathrm{e}}=0.50$.

The turbulence correlation between the fluid velocity and the particle concentration, $\overline{u_i'c'}$, is evaluated by Eq. (35), in which a gradient-type formulation of particle diffusion is adopted. The turbulence Shumidt number of the particle concentration, σ_{c}, in Eq. (35) is taken simply here as $\sigma_{\mathrm{c}}=1.0$.

The coefficient α in Eq. (37) to evaluate P_{G} represents the fraction of the GS energy produced by the drag force due to the relative velocity between the fluid and the particle to be transformed to the SGS energy. Since Kanda and Hino (1994) suggest that this term is closely related to the wake behind the obstacle, α may be strongly affected by the particle Reynolds number R_{ed}. Hetsroni (1989) indicates that the vortex shedding phenomenon behind the particle, which occurs in the range $R_{\mathrm{ed}}>400$, causes the enhancement of the fluid turbulence.

To take account of the effect of the vortex shedding phenomenon on the fluid turbulence, in the present study, the values of 0.1 and 1.0 are given to α in the range $R_{ed} < 400$ and $R_{ed} > 400$, respectively.

Since the GAL model for the particle motion adopts the grid-volume averaging operation, it is easily combined with the SGS model for the fluid turbulence. This is a crucial point to constitute an effective LES model for multiphase turbulence flows. The multiphase LES model so obtained is named here the 'GAL-LES model'.

3. Test of the GAL model for simple convection and diffusion problems

To check the fundamental performance of the GAL model with improved reallocation procedure described in Section 2.3, calculations have been made for simple one-dimensional convective transport and for diffusion. These computations were performed in the x domain of 10,000 m with the grid size Δx of 100 m. The performance of the GAL model with the improved scheme has been examined by comparing with the exact analytical solutions.

3.1. Convection problem

The computation for the convective transport without diffusion, in which a Gaussian or a step distribution of the particle concentration is initially imposed, has been conducted with the constant velocity U of 0.5 ms^{-1}. The peak in the Gaussian distribution is initially located at $x = 0$ with the value of c_0, while the initial distribution of the particle concentration for a step distribution is given as

$$c(0,x) = c_0(x \leq 0), \quad c(0,x) = 0(x > 0) \tag{38}$$

Fig. 8(a) shows the computational results at the computational time steps of 100 for the Gaussian distribution with the different values of $\Delta x/D$, 0.106 and 0.425, where D is the half-width of the Gaussian distribution of the initial particle concentration. The Courant number in this case is 0.5. Although for $\Delta x/D = 0.425$ the normalized particle concentration shows the peak value slightly smaller than unity, the computed c-profiles give almost good agreements with the theoretical values. Fig. 8(b) represents the computational results for the step distribution at 50 time steps for the Courant number of 0.5 and 2.0. The computational results give complete agreements with the theoretical values even for the case of the Courant number greater than unity, indicating that the improved GAL model can exactly simulate the convective translation of a sharp front. These results demonstrate that the improved GAL model has the fundamental performance for convective problems. For further test of the GAL model for a convective problem, one can refer to Nihei and Nadaoka (1998).

3.2. Diffusion problem

A calculation has been performed for a simple linear one-dimensional diffusion process without advection in which a point source with a magnitude M is initially imposed, i.e.

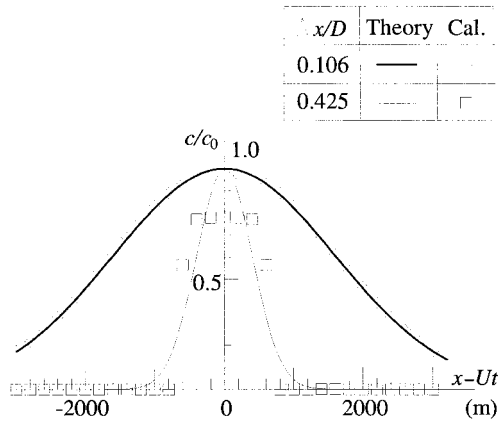

(a) Gaussian distribution

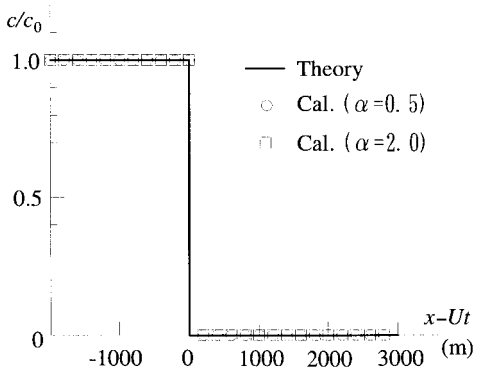

(b) Step distribution

Fig. 8. Performance of the GAL model with the improved reallocation procedure for a one-dimensional convection problem. (a) Gaussian distribution. (b) Step distribution.

$$c(x,0) = M\delta(x) \tag{39}$$

The theoretical expression of the concentration $c(x, t)$ for this problem is

$$c(x,t) = \frac{M}{\sqrt{4\pi\nu_c t}} \exp\left(-\frac{x^2}{4\nu_c t} \right) \tag{40}$$

For the GAL model computation, as the initial condition corresponding to Eq. (39), the uniform particle concentration c_0 is given only within the central grid at $t = 0$, c_0, being $M/\Delta x$. The diffusion coefficient ν_c in Eq. (40) is evaluated from Eq. (18) to be

$$\nu_c = \overline{u_s'^2} T_s \tag{41}$$

and in the present computation 100 cm^2/s^2 and 0.50 s are given for $\overline{u_s'^2}$ and T_s, respectively. An open boundary condition was applied to the both ends of the computational domain. For examining the dependence of the computational result on the time step Δt, the computation was executed with three different time steps, 0.05, 0.10 and 0.50 s.

Fig. 9(a) shows the computed c-profiles at several instants in case of $\Delta t = 0.05$ s and compares them with the theory. The slight discrepancy found near $x = 0$ at $t = 0.25$ s is attributable to the fact that at earlier stage of the computation the representative width of the c-profile is comparable to the grid size Δx, in which the concentration is assumed to be uniform in the GAL model. Except for this slight discrepancy, the computational result shows quite good agreement with the theory. Fig. 9(b) represents the temporal change of the variance of the c-profile computed with the three different computational time steps. The very good agreement of the computational result with the theory, which is indicated with a solid line, is again found regardless of the computational time step. From these results one can confirm the fundamental validity of the GAL model for a diffusion problem.

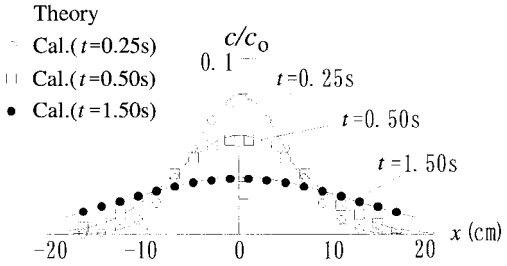

(a) Sequence of spatial distribution of concentration (Δt=0.05s)

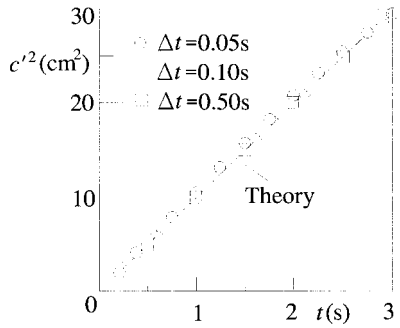

(b) Variance $\overline{c'^2}$

Fig. 9. Performance of the GAL model with the improved reallocation procedure for a one-dimensional diffusion problem. (a) Sequence of spatial distribution of concentration ($\Delta t = 0.05$ s). (b) Variance.

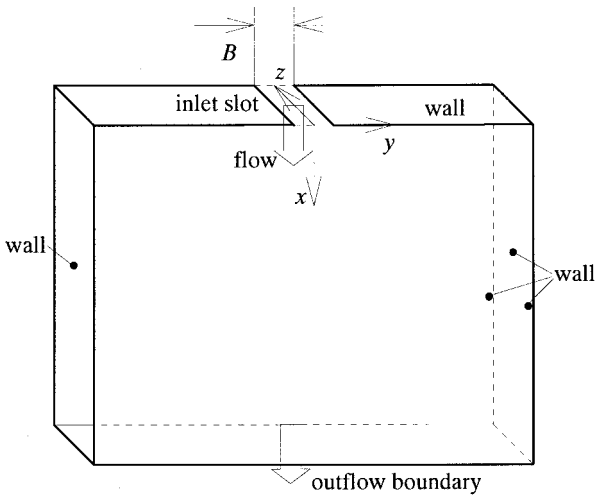

Fig. 10. Definition sketch of computational domain for a particle plume simulation.

4. Computation of a particle plume by the GAL-LES model and discussion

4.1. Computational conditions

The GAL-LES model has been applied to a particle plume which is driven by a constant discharge of the solid particles at an inlet slot into the still water contained in a tank as illustrated in Fig. 10. The computational conditions, as shown in Table 1, correspond to those of the experiment conducted by Tamai and Muraoka (1996).

The computational domain has the dimensions of 60, 60 and 5 cm in the x-, y- and z-directions, respectively, which are defined in Fig. 10. The number of the computational grid points is 60, 40 and 10 in each direction. The velocity components in the x-, y- and z-directions are denoted as u, v and w.

At the inlet boundary, the particle velocity is assumed to be its terminal falling velocity, w_0, and the particle concentration c is then

$$c = q/w_0 B \tag{42}$$

Table 1
Computational conditions

	Case 1	Case 2
Particle diameter d (cm)	0.30	0.10
Specific gravity ρ_s/ρ	2.64	2.64
Terminal velocity w_0 (cm/s)	31.1	15.4
Particle discharge q (cm^2/s)	1.00	1.80

where q denotes the particle discharge rate per unit spanwise length at the inlet slot and B the transverse width of the slot ($=1$ cm). At the outflow boundary located in the lower boundary, the convective boundary condition is employed:

$$\frac{\partial \phi}{\partial t} + U_{CA}(y)\frac{\partial \phi}{\partial x} = 0 \tag{43}$$

where ϕ denotes a variable to be computed, like velocity, pressure and SGS turbulence kinetic energy in the fluid phase. According to Dai et al. (1994), the convection velocity $U_{CA}(y)$ at the outflow boundary is defined as

$$U_{CA}(y) = (C_1 U_{mex} - U_A)\ \exp\left\{ -\left(\frac{y}{C_2 b_{ex}}\right)^2 \right\} + U_A \tag{44}$$

where U_{mex} and b_{ex} are, respectively, the mean velocity at $y = 0$ and the half width of the mean velocity on the outflow boundary. Both the quantities are specified by the experimental results (Tamai and Muraoka, 1996); 20.0 and 30.0 are given to U_{mex} in cases 1 and 2, respectively, and 4.0 to b_{ex} in both cases. The constants C_1 and C_2 and U_A are chosen to be $C_1 = 0.8$, $C_2 = 1.5$ and $U_A = 0.005$ in accordance with Dai et al. (1994). At all the other boundaries, the wall condition is applied. As the initial condition, the still water condition is assumed.

4.2. Computational results and discussion

Fig. 11 shows the spatial distribution of the fluid-phase velocity vector $\mathbf{v}$ and the particle concentration c in the x–y plane ($z = 2.5$ cm) in case of relatively larger particle, case 1. At the beginning stage of the computation, $t = 3.0$ s, the fluid-phase is dragged simply downward by the falling motion of the particles. The spatial distributions of the fluid-phase velocity and the particle concentration are symmetrical along the center line. The fluid-velocity distribution at $t = 5.0$ s is not symmetrical any more and there arise several large eddies in a staggered alignment. These eddies can be regarded as the same kind observed in a usual free-turbulent flow like a jet and plume. The corresponding field of the solid-particle concentration exhibits a characteristic spatial fluctuation pattern with close relation to the motion of the fluid phase. These facts manifest the importance of the large-scale eddies in the turbulent transport process of solid particles. At $t = 6.0$ s, the large-eddy motion in the fluid phase is developed further and the spatial fluctuation of the particle concentration is more noticeable. Since the overall characteristic of the flow pattern after $t = 6.0$ s does not change appreciably, the calculated results after $t = 6.0$ s are not shown here.

Fig. 12 shows the computational results in case of relatively smaller particle diameter, case 2, at $t = 7.0$ s. The main features of the large-eddy formation and the spatial fluctuation of the solid-particle concentration are similar to those for case 1. However, due to more distinct development of the large eddies, there arises more marked asymmetrical distribution of the particle concentration. This is attributed to the fact that the difference in the inertia force depending on the particle diameter causes the difference in the response of the particle motion to the fluid-phase motion.

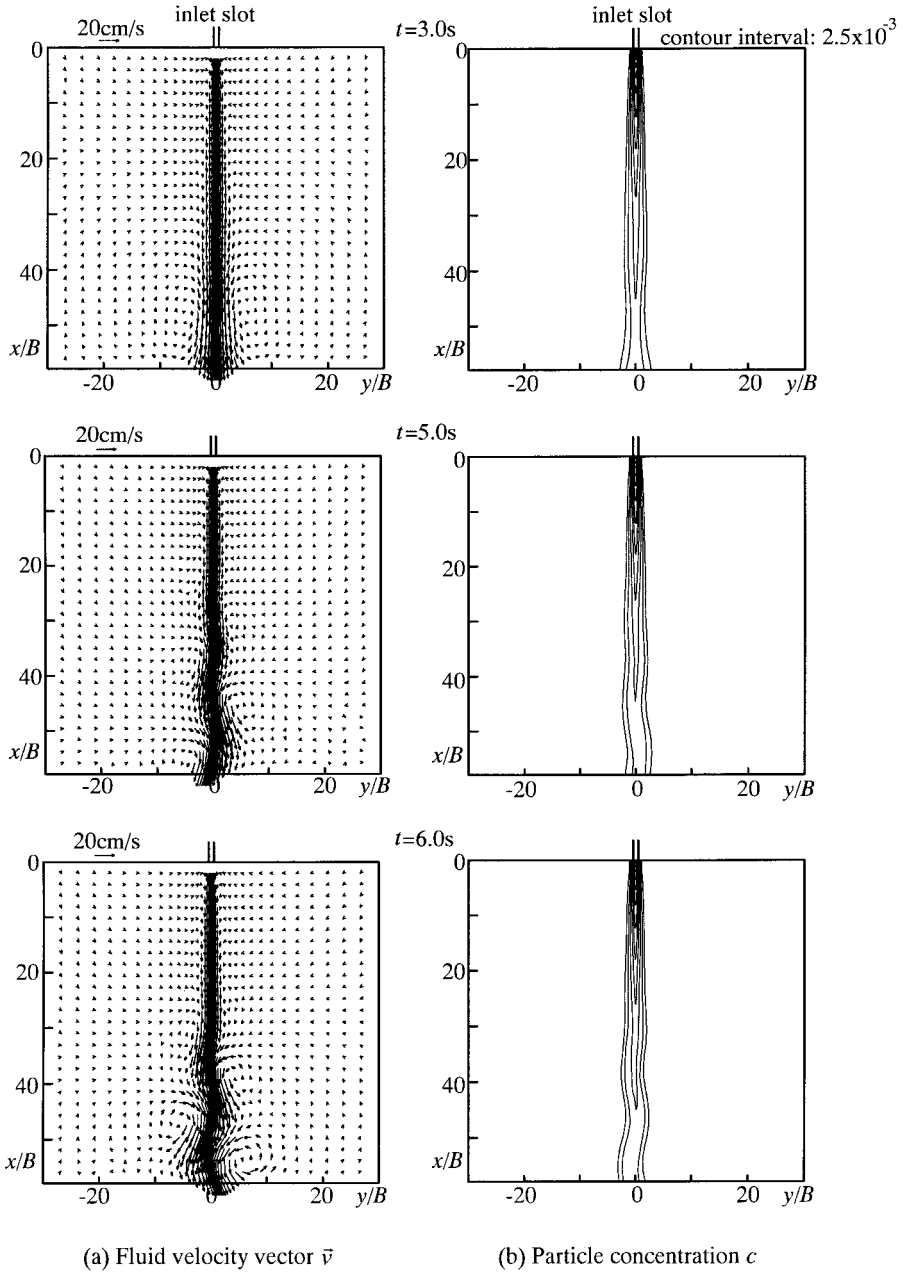

Fig. 11. Spatial distributions of **v** and c in case 1. (a) Fluid velocity vector **v**. (b) Particle concentration c.

Fig. 13 represents the comparison between the computational and experimental results of the lateral distributions of the time-averaged vertical velocities in each phase and particle concentration. The vertical axis denotes the velocities in both phases and the particle concentration normalized, respectively, by the fluid velocity and the particle concentration both

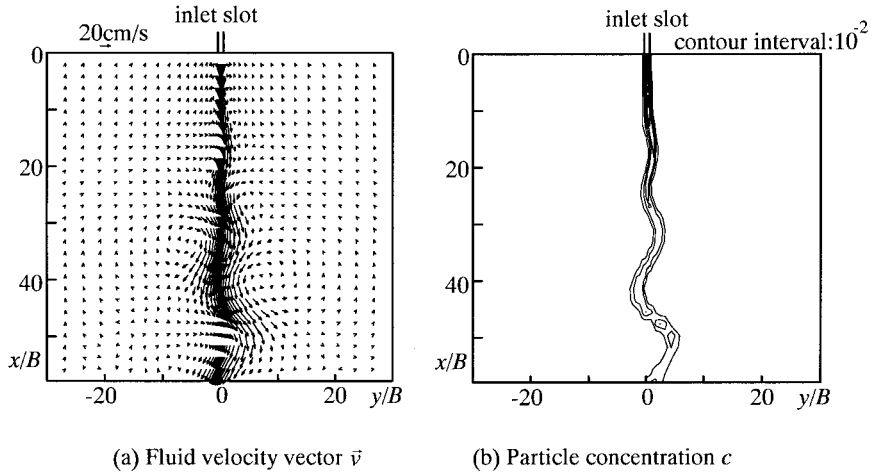

Fig. 12. Spatial distributions of **v** and c in case 2. (a) Fluid velocity vector **v**. (b) Particle concentration c.

at the center line, $\overline{u_c}$ and $\overline{c_c}$. The horizontal axis indicates the distance y from the center line normalized with the half-value width of the fluid-phase velocity, y_h. Since no appreciable difference in the computational results of these normalized values can be found at each cross-section, only the results at $x/B = 25$ are shown here. These figures indicate that the computational results give acceptable agreements with the measured values except for the mean particle velocities in case 2. This discrepancy is considered to be due to the formulation of the drag forces between the fluid and particle phases: that is, the general formulation of the drag force has not been obtained for turbulent flow fields with high particle concentration like case 2 and thus the low accuracy of the drag formulation causes the discrepancy between the experimental and computational particle velocities in case 2. Therefore, for further improvement of the present model, a more accurate evaluation of the drag force relevant to various flow conditions is required.

The downward fluid velocity at the center line, $\overline{u_c}$, and the half-value width of the fluid velocity, y_h, along the center line are represented in Fig. 14. This figure indicates that the calculated values of $\overline{u_c}$ and y_h are well reproduced in both cases.

Fig. 15 depicts the lateral distributions of the time-averaged Reynolds stress in the fluid phase at $x/B = 25$. Since the fluid-phase turbulence, in the present model, is separated into the GS and SGS components, each component of the Reynolds stress is also indicated. The SGS component is evaluated from Eq. (32), that is, multiplying the spatial gradient of the fluid velocity by the turbulent eddy viscosity. These figures show that the computational results give excellent predictions of the Reynolds stress in the fluid phase.

Concerning the relative contribution of the SGS and GS components to the total Reynolds stress, in case 1 the SGS component is more dominant than the GS component, while in case 2 the GS component is more noticeable. These facts agree with the experimental findings by Tamai and Muraoka (1996) that in a particle plume with relatively larger particle diameter like

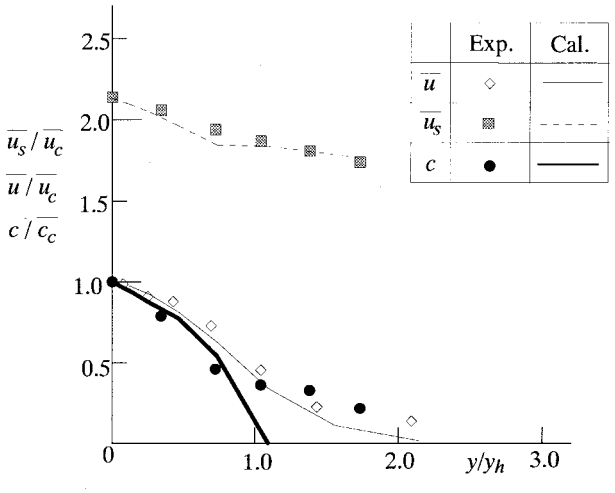

(a) case1

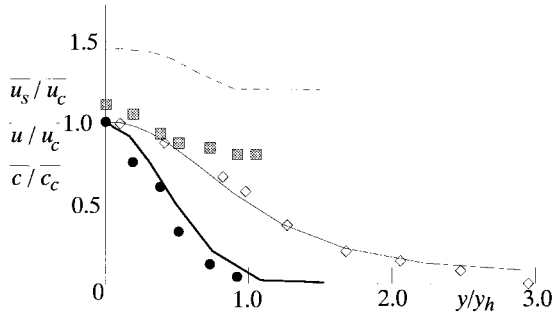

(b) case2

Fig. 13. Transverse distributions of time-averaged particle and fluid velocities and particle concentration. (a) Case 1. (b) Case 2.

case 1 small-scale turbulence corresponding to the SGS component in the fluid phase is dominant, while in case of smaller particle diameter such as case 2 large-eddy motion becomes noticeable. The dependence of the relative significance of the SGS and GS Reynolds stresses on the particle diameter may be explained by the fact that the large-eddy structure in the fluid phase is affected by the difference in the inertia force of the particle motion as described above, and that the production of the SGS turbulence energy is affected also by the relative velocity between both phases.

From the above results, it is concluded that the computational results for the particle plume are in good agreement with the measured, demonstrating the validity of the GAL-LES model.

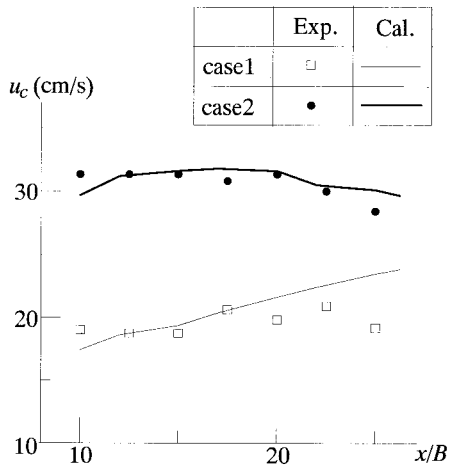

(a) Fluid velocity at the center line, $\overline{u_c}$

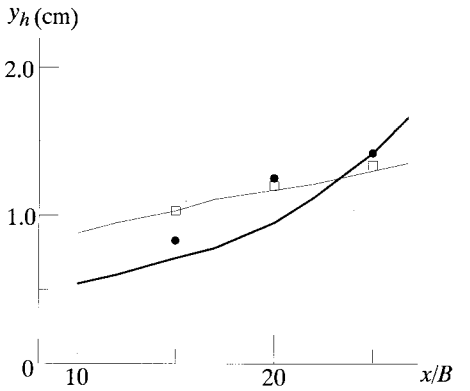

(b) Half-value width of the fluid velocity, y_h

Fig. 14. Time-averaged fluid velocity $\overline{u_c}$ and half-value width y_h along the centerline. (a) Fluid velocity at the center line, $\overline{u_c}$. (b) Half-value width of the fluid velocity, y_h.

5. Conclusions

A new model for dispersed particle motion in multiphase turbulent flow is presented to provide an LES model for multiphase turbulent flow in which a large number of particles are involved. The model for dispersive particle motion, which is referred to here as GAL (grid-averaged Lagrangian) model, is based on an averaging operation for a Lagrangian-type equation of motion of a particle over a computational grid volume and a procedure of

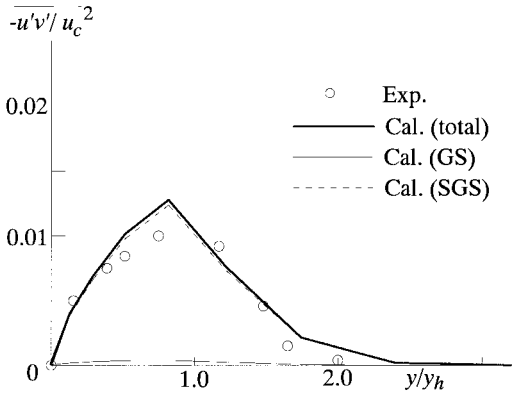

(a) case1

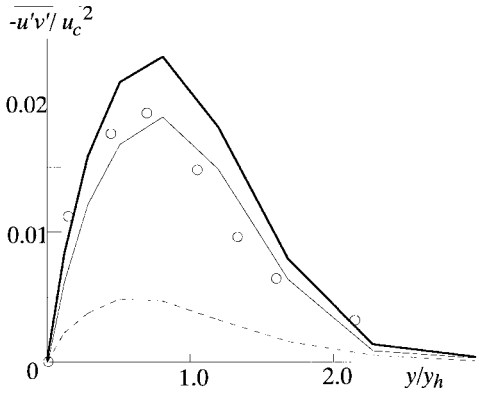

(b) case2

Fig. 15. Transverse distribution of the Reynolds stress in the fluid phase. (a) Case 1. (b) Case 2.

reallocation of a dispersed particle cloud with its centroid movement to each grid. The model is therefore a mixed Eulerian–Lagrangian model which can effectively reduce computational time compared with existing Lagrangian-type models, without losing the advantage of Lagrangian models that they can properly describe the dynamical evolution of particles. Since the GAL model adopts the grid-volume averaging operation it can easily provide an effective SGS model for LES modeling of multiphase turbulent flow. The validity of the multiphase LES model so obtained, which is called here the GAL-LES model, has been confirmed by applying it to a

particle plume computation and comparing with the laboratory data obtained by Tamai and Muraoka (1996). The computation has succeeded in reproducing the large-eddy motion of the fluid phase and the associated spatial fluctuation of the particle concentration. The time-averaged velocities of the fluid and particle phase, the particle concentration and the Reynolds stress in the fluid phase give good agreement with the experimental data, demonstrating the validity of the GAL-LES model. The relative contribution of the SGS and GS components to the total Reynolds stress was found to have appreciable dependence on the particle diameter.

References

Auton, T.R., Hunt, J.C.R., Prud'homme, M., 1988. The force exerted on a body in inviscid unsteady non-uniform rotational flow. J. Fluid Mech. 197, 241–257.

Bird, G.A., 1976. Molecular gas dynamics. Claredon Press, Oxford.

Bouillard, J.X., Lyczkowski, R.W., Gidaspow, D., 1989. Porosity distributions in a fluidized bed with an immersed obstacle. AIChE J. 35, 908–922.

Campbell, C.S., Brennen, C.E., 1985. Computer simulation of granular shear flows. J. Fluid Mech. 151, 167–188.

Chen, C.P., Wood, P.E., 1985. A turbulence closure model for dilute gas-particle flows. Can. J. Chem. Engng 63, 349–360.

Cundall, P.A., 1971. A computer model for simulating progressive, large-scale movements in blocky rock systems. In: International Symposium on Rock Mechanics, Nancy, France, vol. 2, pp. 129–140.

Dai, Y., Kobayashi, T., Taniguchi, N., 1994. Large eddy simulation of plane turbulent jet flow using a new outflow velocity boundary condition. JSME Int. J. 37, 242–253.

Ebert, F., Dehning, C., 1992. Large eddy simulation of turbulent channel flow of dilute suspensions. In: Proceedings of 6th Workshop on Two-phase Flow Predictions, Erlangen, pp. 230–249.

Elghobashi, S.E., Abou-Arab, T.W., 1983. A two-equation turbulence model for two-phase flows. Phys. Fluids 26, 931–938.

Elghobashi, S., Abou-Arab, T., Rizk, M., Mostafa, A., 1984. Prediction of the particle-laden jet with a two-equation turbulence model. Int. J. Multiphase Flow 10, 697–710.

Hetsroni, G., 1989. Particles-turbulence interaction. Int. J. Multiphase Flow 15, 735–746.

Hinze, J.O., 1975. Turbulence. McGraw-Hill, New York.

Kanda, M., Hino, M., 1994. Organized structures in developing turbulent flow within and above a plant canopy, using a large eddy simulation. Boundary-Layer Meteorol. 68, 237–257.

Kitron, A., Elperin, T., Tamir, A., 1990. Monte Carlo simulation of gas-solids suspension flows in impinging streams reactors. Int. J. Multiphase Flow 16, 1–17.

Marble, F.E., 1970. Dynamics of dusty gases. Ann. Rev. Fluid Mech. 2, 397–446.

Mols, B., Oliemans, R.V.A., 1998. A turbulent diffusion model for particle dispersion and deposition in horizontal tube flow. Int. J. Multiphase Flow 24, 55–75.

Nadaoka, K., Nihei, Y., Yagi, H., 1995. A new framework for LES modeling of solid-liquid phase turbulent flow—a mixed Euler–Lagrangian approach. Proceedings of 2nd International Conference on Multiphase Flow, Kyoto, vol. 2, pp. 71–74.

Nihei, Y., Nadaoka, K., 1998. Improvement of GAL model for convective transport simulation. In: Proceedings of 3rd International Conference on Multiphase Flow, CD-ROM.

Nihei, Y., Nadaoka, K., Yagi, H., 1997. Large-eddy computation of horizontal fluidized bed by a new multiphase LES. In: Coastal Dynamics '97, pp. 1053–1061.

Squires, K.D., Eaton, J.K., 1990. Particle response and turbulence modification in isotropic turbulence. Phys. Fluids A 2, 1191–1203.

Squires, K.D., Eaton, J.K., 1991. Measurements of particle dispersion obtained from direct numerical simulations of isotropic turbulence. J. Fluid Mech. 226, 1–35.

Tamai, M., Muraoka, K., 1996. On turbulence properties of particle plumes. In: Proceedings of 26th Congress of International Association for Hydraulic Research, vol. 2, pp. 202–207.

Tanaka, T., Kiribayashi, K., Tsuji, Y., 1991. Monte Carlo simulation of gas-solid flow in vertical pipe or channel. In: Proceedings of International Conference on Multiphase Flows '91-Tsukuba, vol. 2, pp. 439–442.

Tchen, C.M. 1947 Mean value and correlation problems connected with the motion of small particles suspended in a turbulent fluid, Ph.D. thesis, University of Delft, Martinus Nijhoff, the Hague.

Uchida, Y., Hakuno, M., 1990. Distinct element analysis of dry rock avalanches. Proc. Jap. Soc. Civil Engnrs 422, 85–96.